A new remote predictor of wave reflection based on runup asymmetry

Rafael Almar[1], Chris Blenkinsopp[2], Luis Pedro Almeida[3], Patricio A. Catalán[4,7,8], Erwin Bergsma[1,3], Rodrigo Cienfuegos[5,7] and Nguyen Trung Viet[6]

Abstract

Reflected waves account for a significant part of the nearshore energy budget and influence incoming waves, nearshore circulation and sediment transport. The use of swash parameters to estimate wave reflection is investigated at three different beaches ranging from highly reflective to dissipative. It is observed that it is essential to account for swash processes when estimating reflection, in particular at intermediate and reflective beaches with a steep beachface. Our results show that runup asymmetry in uprush/backwash can be used as a proxy for dissipation in the swash zone: larger asymmetry values indicating greater dissipation. In our dataset, a reflection predictor based on runup asymmetry has better skill in comparison to empirical predictors based on surf similarity, because runup is a process that integrates both surf and swash zone wave transformation. Runup asymmetry behaves as a swash similarity parameter and reflects an equilibrium between swash period, slope and dissipation.

Keywords: Nearshore; video imagery; runup asymmetry; swash dissipation; reflection

Highlights:

- Link between swash parameters and wave reflection investigated at three different beaches
- Asymmetry in uprush/backwash can be considered a proxy for swash dissipation
- Evidence of equilibrium between runup asymmetry, period and slope

[1] IRD-LEGOS, Toulouse, France
[2] Water, Environment and Infrastructure Resilience Research Unit, University of Bath. Bath, UK
[3] CNES-LEGOS, Toulouse, France
[4] Dpt Obras civiles-Universidad Tecnica Federico Santa Maria, Valparaiso, Chile
[5] DIHA-Pontificia Universidad Catolica de Chile, Santiago, Chile
[6] Thuyloi University, Vietnam, Hanoi, Vietnam
[7] Centro Nacional de Investigación para la Gestión Integrada de Desastres Naturales, CONICYT/FONDAP/1511007, Santiago, Chile
[8] CCTVal-Centro Científico Tecnológico de Valparaíso, Valparaíso, Chile.

1. Introduction

Field and laboratory studies have demonstrated that incident wave energy is not entirely dissipated when it reaches the shoreline. Part of the incident wave energy is reflected into deeper water (Mansard & Funke, 1980; Miche, 1951; Tatavarti, Huntley, & Bowen, 1988). As a rule-of-thumb: the steeper the beach, the more incident wave energy is reflected, and vice versa. At the steepest beaches and in the case of long period waves, observations show that up to 60-80% of the incoming wave energy is reflected (Battjes, 1974; Elgar et al., 1994). Reflected waves can strongly influence and interact with incident waves; change individual wave shape (Abdelrahman and Thornton, 1987; Rocha et al., 2017), intensify undertow (Martins et al., 2017), and generate standing or even resonant waves (Almar et al., 2012; 2016). This effect on the hydrodynamics is thought to have a feedback on submerged morphological bed forms (e.g. O'Hare and Davies, 1993; Hancock and Mei, 2008), and can also modify offshore wave conditions. In deep water up to 15% of the total wave energy can be linked to coastal reflection (Ardhuin and Roland, 2012) as reported in the Gulf of Guinea, West Africa (Laibi et al., 2014), where beaches are generally steep and incident waves are long. Hence, it is crucial to understand and accurately predict reflection at natural beaches.

Based on the laboratory study of Iribarren and Nogales (1949), Battjes (1974) demonstrated that wave reflection is proportional to a "surf similarity" parameter ξ which quantifies surf zone conditions:

$$\xi = \frac{\tan(\alpha_f)}{\sqrt{H/L_0}} \qquad \text{(Eq. 1)}$$

where α_f is the foreshore slope, and H and L_0 are the wave height and deep-water wavelength respectively. Dissipative conditions are generally associated with low values of ξ, typically less than 0.3 (Stockdon et al., 2006; Ruggiero et al., 2001; Ruessink et al., 1998, Raubenheimer and Guza, 1996; Raubenheimer et al., 1995; Guza and Thornton, 1982), whereas intermediate and reflective conditions are associated with larger values (Holland and Holman, 1999; Holland, 1995; Holman, 1986; Holman and Sallenger, 1985). The surf similarity equation provides satisfactory reflection estimates for gentle slopes (low ξ) when dissipation is dominated by wave breaking, but overestimates reflection for $\xi > 2.5$, when wave energy dissipation in the swash zone becomes more significant (Ahrens, 1979; Seelig and Ahrens, 1981; Sutherland and O'Donoghue, 1998; Baldock, P. Holmes, 1999). Furthermore, the surf similarity parameter is a seemingly weak proxy for reflection in the case of complex bathymetries such as two-slope profiles (Mizuguchi, 1984; Elgar et al., 1994; Davidson et al., 1996; Miles & Russell, 2004). Field and laboratory data (e.g. Dickson et al., 1995; Inch

et al., 2016) indicate that reflection is primarily proportional to the wave period and the effect of wave height is negligible.

Muttray et al. (2006) indicate that reflection predictors based on ξ overestimate the effect of wave breaking, and highlight the potential role of swash zone dynamics when predicting reflection. But, while the description of reflection in terms of surf zone conditions has attracted a lot of attention, literature describing wave energy reflection in terms of swash dynamics is rather limited. Guedes et al (2011) observed no link between swash energy and ξ, implying that swash energy and wave reflection are independent at the hourly scale. However, Martins et al. (2017) found a correlation between peak swash potential energy and reflected wave energy at the time-scale of individual waves on a steep, reflective, large-scale laboratory beach, suggesting that reflected waves energy can be predicted based on detailed swash measurements.

Swash is far from a simple oscillation of the waterline. Whitham (1958) and Shen & Meyer (1963) introduced a parabolic ballistic approach for run-up as a solution for a collapsing bore running over a dry beach. Hughes et al. (1997), Guard & Baldock (2007) and Power et al. (2011) showed in the field and with laboratory measurements that swash flow can be far from symmetric, with the antagonistic effects of wave energy and gravity over beach slope. On the other hand, Guza & Bowen (1976) depict the swash as the antinode of a standing wave for non-breaking waves, with a rather symmetric runup shape. Observations show that runup asymmetry results predominantly from the effect of bore dissipation during the uprush, which occurs mainly due to breaking and friction (Hughes & Fowler, 1995; Puleo & Holland, 2001), and this includes the influence of sediment grain size (Masselink & Hughes, 1998, Elfrink & Baldock, 2002) but also swash-swash interactions (Baldock & Holmes, 1999; Hughes & Moseley, 2007); catch-up and absorption during the uprush, and collision between uprush and the preceding backwash (Chen et al., 2016). Large values of runup asymmetry are thought to indicate large dissipation and weak reflection. Because the measurement of reflection and swash is a difficult task in the field, observations are scarce. Nonetheless, current remote sensing techniques such as video imagery (Power et al., 2011; Almar et al., 2017) or LiDAR (Blenkinsopp et al., 2010) are capable of obtaining suitable data.

This paper stresses the role played by swash in controlling reflection, which is ignored in most common predictors based on surf zone conditions. A predictor for wave reflection based on swash asymmetry is introduced and validated using datasets collected at three contrasting natural beaches covering a range of conditions from dissipative to highly reflective. We investigate the advantage of using swash dynamics for predicting reflection rather than the surf similarity parameter ξ, in

particular at complex beaches and hourly timescales. Finally, the role of asymmetry to indicate "swash similarity" is discussed and some concluding remarks are provided.

2. Data and methods

Data were collected during three experiments undertaken in 2012-2013 at three different field sites (Figure 1), ranging from dissipative to reflective beach slopes and low to high energetic wave conditions. The corresponding hydro-morphological conditions during the three experiments are shown in Figure 2.

A dissipative beach (upper beach slope α=0.05) experiment was conducted at Mataquito, Chile, from November 28th to December 14th, 2012 (Cienfuegos et al., 2014). Mataquito is a medium grain-sized (D_{50} = 0.2 mm), alongshore uniform, barred beach with a micro-tidal range and a wave climate dominated by swell waves (annual mean derived from EraInterim -ECMWF, Dee et al., 2011- for the 1979-2012 period, $H_s \sim$ 2.4 m, $T_p \sim$ 12 s, SW). During the experiment, tidal amplitude ranged from 0.4 to 1 m. A large swell hit the coast on Dec. 2, (H_s = 4m, T_p = 18 s, day 3 in Fig. 2, left panels), followed by moderately energetic conditions starting on Dec. 5 (H_s = 1-2 m, T_p = 10-15s).

An intermediate beach (upper beach slope α=0.12) experiment was conducted at Nha Trang, Vietnam, from December 3rd to 10th, 2013 (Lefebvre et al., 2014). Nha Trang is a uniform low-tide terrace, medium grain-sized (D_{50}=0.3 mm) beach with a micro-tidal range and a low to moderate energy wave climate (annual mean, H_s < 1 m, T_p < 5 s, E). During the experiment, tidal amplitude decreased from 1.2 to 0.5 m. Wave height and period decreased continuously, from H_s = 1m, T_p = 9 s to H_s = 0.5m and T_p = 5 s.

A reflective beach (upper beach slope α=0.15) experiment was conducted at Grand Popo, Benin, from February 17th to 28th, 2013. Grand Popo is a reflective, medium to coarse grain-sized (D_{50} = 0.6 mm), alongshore uniform, low-tide terraced beach with a micro-tidal range and a wave climate dominated by swell waves (annual mean, $H_s \sim$ 1.4 m, $T_p \sim$ 9.4 s, SW) (Almar et al., 2014a). During the experiment, tidal amplitude increased from 0.5 m to 1.4 m. An energetic swell hit the coast on Feb. 23, (H_s = 1.5 m, T_p = 18 s), followed by moderate conditions.

At each site, the upper beach slope was extracted from daily topographic surveys undertaken at low tide using differential GPS. Directional wave measurements were obtained in approximately 10 m water depth (red circles in Fig. 1) using an Acoustic Doppler Current Profiler (ADCP Workhorse Sentinel 1200 KHz, 20-min wave bursts; see method in Jeans et al., 2002). Shore-based video swash monitoring was undertaken at 2 Hz during daylight hours at the three experiment sites. Time series of pixel intensity sampled along a cross-shore line (time stacks) (Holland & Holman, 1993) were

collected to measure wave runup, which was detected by applying a Radon Transform (RT) approach described in Almar et al. (2017). In this study, the ability of the RT to detect the instantaneous shoreline was assessed by comparison to concurrent LiDAR measurements and compared to the commonly used color contrast method (CC), which defines the waterline from RGB colorband contrast. Because the RT is based on motion detection it is more able than the CC approach for distinguishing between backwash and the groundwater seepage line, and is less sensitive to poor light conditions. Rectification of images from pixels into real-world coordinates was accomplished by direct linear transformation using DGPS ground control points (Holland et al., 1997) after a correction of the radial lens distortion (Heikkila & Silven, 1997). Although varying somewhat throughout the field of view, the pixel footprint was less than 0.1 m in the cross-shore direction over the region of interest (surf-swash zones). A single cross-shore transect was considered at the three sites, assuming alongshore-uniform processes, which will not be the case in the presence of longshore variability in the swash dynamics induced by irregular features such as crescentic sandbar (Nicolae Lerma et al., 2017) and beach cusps (Almar et al., 2018).

Swash energy flux F_{swash} was computed from 1-hr video time stacks (Power et al., 2011; Guedes et al., 2011; Senechal et al., 2011):

$$F_{swash} = E_{swash} C_{gsw} \sim \frac{\rho g R_{sw}^2}{16} \quad \text{(Eq. 2)}$$

Where ρ is water density (here 1025 kg/m^3) and R is the horizontal runup computed from horizontal waterline timeseries S, $R_{sw} = 4(S \tan \alpha_{sw})$, using the RT (Radon Transform method, see Almar et al., 2017) and α_{sw} as the active swash slope, which is defined by Holland and Puleo (2001) as the dynamic slope within the swash zone which changes with tide. A constant shallow water group velocity is considered hereafter $C_{gsw} = \sqrt{gh} \sim 1\ m/s$, using an arbitrary depth of 0(10 cm) at swash inception, due to the lack of information. The directional wave spectra *Ed (θ,f)* were computed from an ADCP (Acoustic Doppler Current Profiler from RD Instrument), using the WavesMon software (see the manual) and the procedure described by Krogstad et al. (1988) and Strong et al. (2000). ~~Incoming and reflected wave energy and direction were computed from co-localized pressure and current measurements from an ADCP (Acoustic Doppler Current Profiler, e.g. Sheremet et al., 2001).~~ Though this technique is commonly used and offers good skill in retrieving swell band waves in intermediate to shallow depths (Herbers and Lentz, 2010), it can have some difficulty in capturing short wind waves due to the attenuation of the wave orbital motion with depth. Several methods exist to separate incoming and outgoing waves; the PUV temporal (e.g. Guza et al., 1974) and spectral

(Sheremet et al., 2002) methods, using pressure and velocity sensors, and array methods that only use cross-shore array of pressure sensors (or any free surface measurements), such as the recent method based on the Radon Transform developed by Almar et al., (2014b). Here, ~~Incoming~~ incoming and outgoing wave heights were ~~defined~~ separated ~~using~~ from *Ed (θ,f)* ~~the ADCP spectra~~following the method described by Sheremet et al. (2002), integrating from the lower to upper cut-off frequency (range set to gravity-infragravity band 0.02 Hz-0.5 Hz) ~~, based on the local shore-normal direction~~:

$$H_{inc} = 4\left(\int_{0.02\ Hz}^{0.5Hz}\int_{-90°}^{90°} E_d(\theta,f)d\theta df\right)^{1/2} \quad \text{(Eq. 3)}$$

$$H_{out} = 4\left(\int_{0.02\ Hz}^{0.5Hz}\int_{270°}^{90°} E_d(\theta,f)d\theta df\right)^{1/2} \quad \text{(Eq. 4)}$$

With $E_d(\theta, f)$ denoting the energy density and the term inside the parentheses representing the variance associated with the defined frequency band and the incidence angle from the shore-normal direction (see also Almar et al., 2014b). Peak period T_p is calculated as the inverse of the peak frequency in $E_d(\theta, f)$. Offshore incoming and reflected wave fluxes, F_{inc} and F_{ref} are computed as $F = ECg = \rho g {H_s}^2 T_p/32\pi$ $(W.m^{-1})$ at the ADCP (depth~10m at the three sites), *Cg* ~~assuming~~ being computed with linear theory using intermediate depth conditions~~deep water conditions for convenience, even if long waves might be slightly shoaling at ADCP locations during energetic conditions~~. Reflection is quantified as the ratio of reflected and incoming energy. At all sites, the ADCP was moored sufficiently far offshore to avoid reflection coefficient variability associated with the surf zone, as described by Baquerizo et al. (1997).

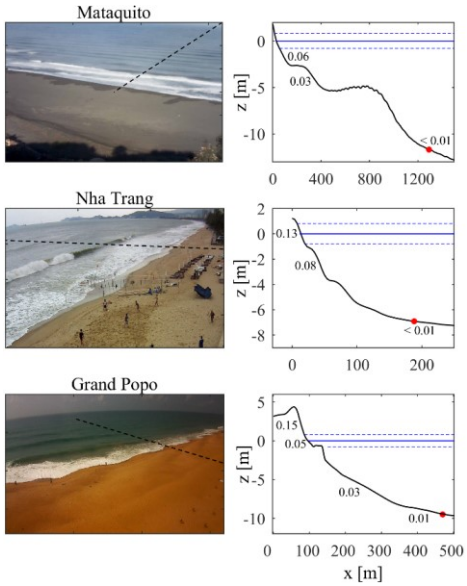

Figure 1: Snapshots from video systems (left) and (right) bathymetry profiles, (top) Mataquito, (mid) Nha Trang, and (bottom) Grand Popo. In the left panels, dashed black lines indicate the cross-shore time stack locations. In the right panels, numbers are local beach slopes, the red circles, solid and dashed blue lines indicate the location of the ADCP, mean sea level, max and min spring tidal elevations, respectively.

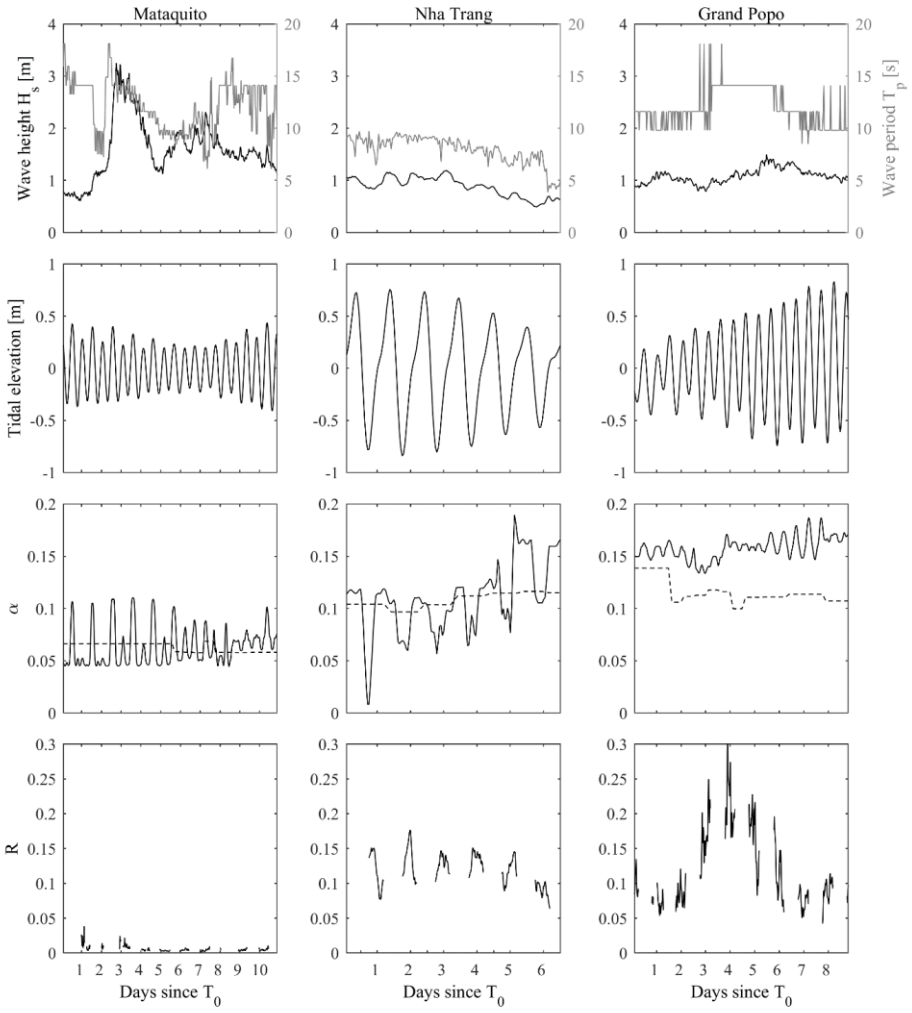

Figure 2: From left to right, Mataquito, Nha Trang and Grand Popo experiments. (Row 1) offshore significant wave height (H_s – black line) peak period (T_p – grey line), (Row 2) tide, (Row 3) shoreface slope α with (active swash slope, solid line) or without (dashed line) tidal modulation. (Row 4) reflection (R).

3. Results

3.1. Nearshore wave energy budget

It is hypothesized that it is essential to account for swash processes when estimating R and the nearshore energy balance, in particular at reflective or complex beaches. This is investigated here through the decomposition of the nearshore wave energy budget (e.g. Baquerizo et al., 1998; Carini et al., 2015). The nearshore wave energy budget (e.g. Sheremet et al., 2001) may be expressed as:

$$F_{inc} - F_{ref} = D_{surf} + D_{swash} \quad \text{(Eq. 5)}$$

With F_{inc} and F_{ref} the offshore incoming and reflected wave fluxes, D_{surf} and D_{swash} the wave dissipation in the surf and swash zone respectively. We assume hereafter that reflection occurs only in the swash zone, with the reflection from submerged bars considered to be negligible (for now) and incident waves sufficiently shore-normal to be reflected back offshore and not get trapped (only leaky modes). Swash energy flux F_{swash} computed in Eq. 2 can also be considered as:

$$F_{swash} = D_{swash} + F_{ref} \quad \text{(Eq. 6)}$$

Eq. 6 can only be satisfied under the assumption that reflected waves do not break when propagating offshore and hence no energy is lost. Figure 3 shows the hourly evolution of D_{swash}, F_{ref} and D_{surf}. F_{inc} and F_{ref} are measured at the ADCP (see Data and Methods Section) and D_{swash} is computed from Eq. 6, D_{surf} is computed from the combination of Eq. 5 and 6. Figure 3 shows that the relative contribution of D_{swash} increases with beach gradient. It is as small as 2 % at Mataquito, increases to 23 % at Nha Trang and up to 35 % at Grand Popo with the reflection coefficient R increasing in a similar manner with values of 1%, 10% and 15 % respectively. As observed by Elgar et al. (1994) and Miles and Russell (2001) R values are generally higher during high tide which is consistent with higher reflection from a steeper beach face. At the two most reflective beaches, Grand Popo and Nha Trang, the dissipation in the swash zone is important, due to the limited wave breaking over the narrow terrace, in particular at high tide as also observed by Miles & Russell, (2004). Under such conditions, swash plays a major role in governing the amount of reflected energy, as shown recently by Martins et al., (2017). In contrast, dissipative beaches such as Mataquito are dominated by breaking processes (Guedes et al., 2011), with minimal influence from the tide level.

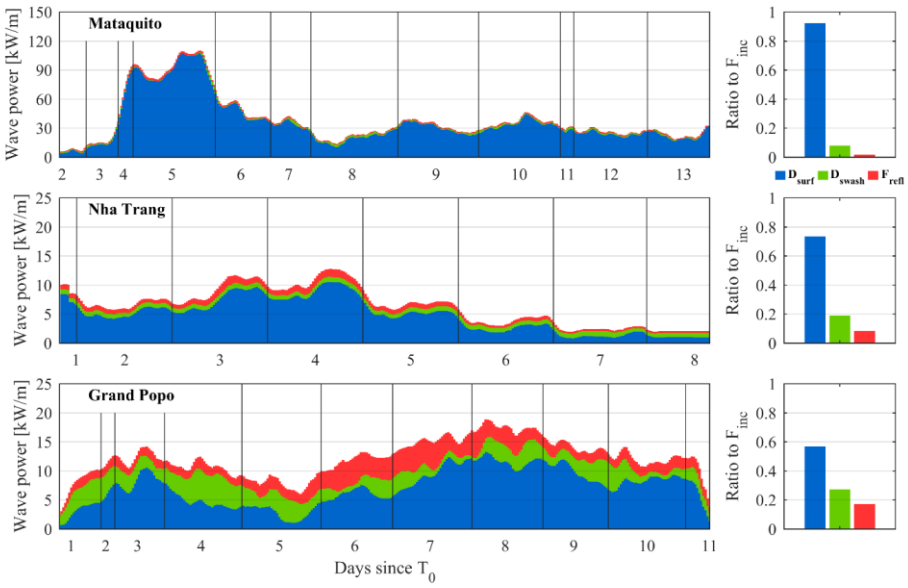

Figure 3: Left panels show a decomposition of the incoming wave power F_{inc} separated into surf zone dissipation D_{surf} (blue) from the combination of Eq. 5 and 6, swash zone dissipation D_{swash} (green) from Eq. 6, and reflected wave energy flux F_{ref} (red). The percentage contribution of each component to the total energy flux is shown in the right panels.

3.2. Wave reflection from runup asymmetry

Reflection measurements typically require the installation of instrumentation in intermediate water depths. The ability to estimate reflection based on swash characteristics would be beneficial and makes in-situ instrumentation redundant. We hypothesize here that D_{swash} is proportional to F_{swash} with $D_{swash} = K\,F_{swash}$ where K is an empirical coefficient that represents swash dissipation:

$$K = (F_{swash} - F_{ref})/F_{swash} \quad \text{(Eq. 7)}$$

Laboratory measurements in the swash zone supported by numerical modelling such as in Martins et al. (2017) estimate the bulk of energy reflected from the beach. A 0.5 coefficient of proportionality was found between reflected bulk and swash energy.

In accordance with the notion of surf similarity, a long wave on a mild slope would represent comparable hydrodynamic conditions as a short wave and a steeper slope (Battjes, 1974). In other words, a given swash slope appears steeper to longer waves than it does to shorter waves. As observed for runup on rubble mound by several authors (e.g. Davidson et al., 1996), on a steeper slope, more energy will be reflected (i.e. less energy will be dissipated). By contrast, a short wave on a flat beach will dissipate its energy through bore breaking-induced turbulence and bottom friction in the uprush which results in a thin layer of weak return flow during the backwash phase of the swash cycle.

Figure 4 illustrates the contrasting swash shapes observed at the three sites. At Mataquito, the runup time series presents a sawtooth shape; the already broken bore (Guard and Baldock, 2004) in combination with a gentle swash slope leads to almost complete energy dissipation during the uprush with a weak backwash. In contrast, at more reflective beaches, such as Nha Trang and even more so at Grand Popo, large bores collapse at the shoreline and the steeper slope leads to strong backwash which seemingly generates significant reflected wave energy (Martins et al., 2017). The variability in uprush/backwash flows discussed above is characterized here through the front-to-lee (temporal) asymmetry (see Elgar and Guza, 1985):

$$As = \frac{\langle H^3(S-\bar{S})\rangle}{\langle (S-\bar{S})^2\rangle^{3/2}} \qquad \text{(Eq. 8)}$$

Where H denotes the Hilbert transform and S represents the horizontal swash excursion, <> indicates time averaging. Figure 4 shows an illustration of different swash conditions with the corresponding runup asymmetry values ranging from pitched forward, dominated by uprush (As=0.71) at Mataquito, to almost symmetrical (As=0.12) at Grand Popo.

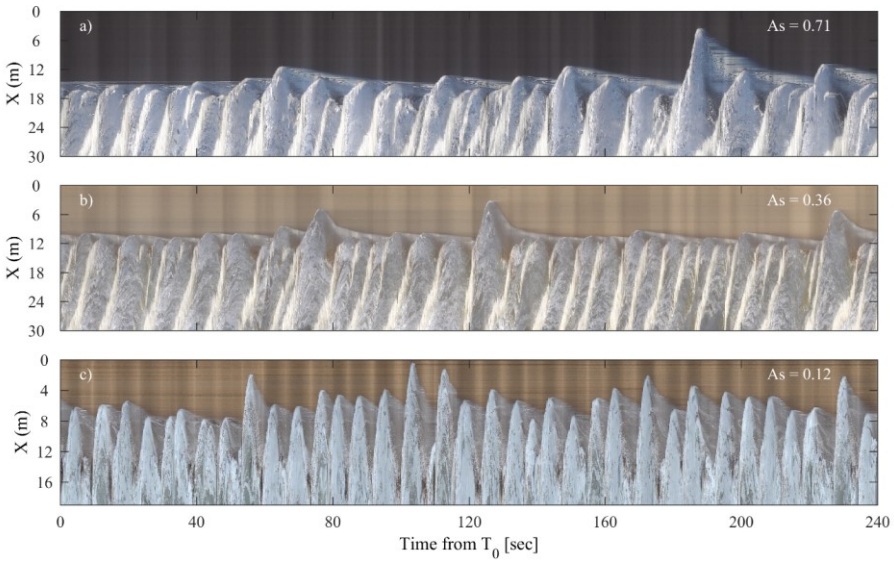

Figure 4: Illustration of video time stacks of the swash zone with asymmetry values at dissipative Mataquito (top), intermediate Nha Trang (mid) and reflective Grand Popo beaches (bottom).

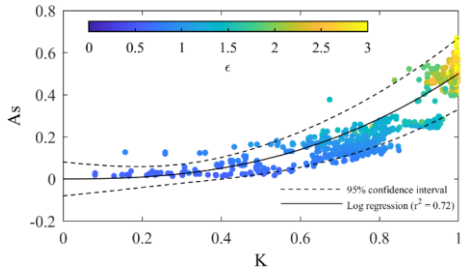

Figure 5: Hourly runup asymmetry *As* (Eq. 8) (computed from the three datasets) as a function of the swash dissipation parameter *K* (Eq. 7). Colours represent the Miche swash similarity parameter ε ($\varepsilon = S\frac{\omega^2}{g}\alpha_{sw}$, where S is the horizontal swash excursion, α_{sw} is the active swash slope, g is the acceleration due to gravity and ω is the angular wave frequency $2\pi/T$ with the swash period T). The solid line is a logarithmic regression and dashed lines show the 95% confidence intervals.

In Figure 5, the aggregate of all of the data collected from the three sites is presented in terms of the swash reflection parameter, the corresponding swash similarity parameter (colour) and the

estimated asymmetry. It can be noted that there is a positive correlation between swash asymmetry and swash dissipation. A functional form can be obtained as:

$$K = aAs^b \quad \text{(Eq. 9)}$$

Where logarithmic best fit regression gives a=1.3 and b=0.4 (significant at 95% level, Figure 5). It is now possible to estimate the reflection coefficient directly as a function of the remotely sensed swash asymmetry:

$$R_{As} = \frac{F_{swash}(1-K)}{F_{inc}} \quad \text{(Eq. 10)}$$

Figure 6 indicates a strong relationship between hourly R_{As} and reflection observed offshore R_{adcp}, with a coefficient of determination of 0.72 (significant at 95% level). Method skill worsens for low reflection values as the Mataquito data is clustered with no clear dependence on As (see Figure 5). However, this swash-based predictor offers a better result for these three datasets than conventional predictor based on surf conditions (following the surf similarity parameter $R_\xi = 0.1\xi^2$, with R^2 = 0.38).

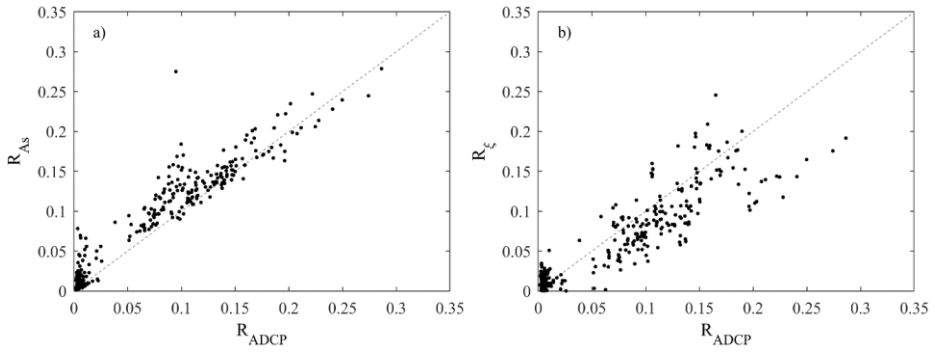

Figure 6: Predicted hourly reflection coefficients from a) runup asymmetry R_{As} and b) conventional predictor based on surf conditions using Battjes's formula $R_\xi = 0.1\xi^2$, as a function of observed reflection coefficient from ADCP R_{adcp}. Dashed lines show 1:1 agreement.

4. Discussion

Runup asymmetry is an all-encompassing parameter that is the result of surf and swash zone wave transformation, and their interaction with morphology. The strongest agreement between asymmetry and wave reflection is found at the most reflective Grand Popo and Nha Trang beaches. This relationship weakens at the dissipative Mataquito beach, where the dependence of reflection on swash dynamics also weakens (see the surf scaling parameter, Guza and Inman, 1975). In such a case, the reflection can be scaled more appropriately using deep-water parameters (Guza & Thornton, 1982; Diaz-Sanchez et al., 2013). The results show that a swash-based reflection proxy is less accurate at dissipative beaches, where runup asymmetry may not be the key controlling factor, or the noise in the reflection data is large compared to the signal itself. This is in line with the observation of Guedes et al., (2011). While the newly developed runup asymmetry predictor is clearly advantageous in comparison with other predictors at two-slope beaches (i.e. different swash and surf slopes) it might be affected by the presence of a submerged sandbar such as observed at Mataquito. Irregular morphological features, such as sandbars, can also introduce multiple reflecting and energy dissipating features (Davies, 1982; Mei, 1985; Bailard et al., 1992; Elgar et al., 2003; Almar et al., 2018) which inherently weakens the link between swash dynamics and offshore waves. Waves transmitted over the bars may undergo partial reflection at the shoreline (Miche, 1951; Elgar et al., 1994), followed by re-reflections from the bars, complicating the wave transformation (Yu and Mei, 2000). Noteworthy, the scatter observed in Figure 6 can be partly attributed to the noise in F_{ref} and F_{inc} estimated at the ADCP. As described in Section 2 (Data and methods), the ADCP can have difficulties to retrieve waves at the lower and upper cut-off frequencies, in particular in capturing short wind waves (e.g. Nha Trang) in relatively deep water and longest waves (e.g. Mataquito).

Identifying the backwash leading edge is notoriously difficult from video imaging and much can be left up to interpretation as the leading edge infiltrates into the bed (Vousdoukas, 2014). The RT method (Almar et al., 2017) is based on motion (i.e. flow) detection rather than colour contrast used in pioneering studies of Holland & Holman (1993) and Holland et al. (1995, 2001). Whereas no substantial differences are expected in terms of swash statistics, the RT might be more suited when studying swash shape, such as asymmetry, as it describes main flow behaviour rather than the behaviour of a weak backwash flow. Most swash models, for example, the ballistic approach of Shen et Meyer (1963) do not account for swash asymmetry and the influence of swash interactions (Bergsma et al., 2018) on the characteristics of the shoreline motion. This is because these sources of energy loss predominately occur seaward of the instantaneous shoreline through the interaction of the incoming bore with the preceding backwash (Baldock and Holmes, 1999). Our data shows that

runup shape, which reflects the level of dissipation, can vary substantially; part of this observed variability could be attributed to the dissipation resulting from these swash interactions (Baldock & Holmes, 1999; Hughes & Mosseley, 2007; Brocchini and Baldock, 2008). While the long period swell waves and steep beach at Grand Popo were observed to lead to minimal interactions, interactions were common at Mataquito. The long-duration return flow of short waves over flat beaches has the potential to enhance swash-swash interaction, dissipating energy and promoting an asymmetric shape.

The normalized swash slope parameter (Battjes et al., 2004) suggests that swash dynamics is primarily influenced by wave period and active swash slope , and thus potentially runup asymmetry *As*. Following the approach in Martins et al., (2017), the range of *As* values for different swash slopes and periods is investigated on an individual swash basis. In Figure 7, the distribution of *As* averaged over the three experiments is presented as a function of swash slope α and swash frequency ω. *As* decreases with α and increases with ω: for a given slope, shorter swashes tend to have higher dissipation (strong *As*) while longer swashes reflect more energy (weak *As*). In a similar manner to the estimation of reflection from the combination of *As* and runup excursion length, this suggests that *As* and ω could be used to estimate swash slope remotely. Because swash hydrodynamics adapt more rapidly than morphology to rapidly varying offshore conditions, there is the potential for high-frequency As and subsequent reflection to provide a short-term predictor of beach slope evolution, though further analysis is required to confirm this.

This new reflection predictor based uniquely on swash dynamics offers the potential to estimate reflection using shore-based remote sensing systems such as video cameras. These tools enable inexpensive and relatively simple long-term monitoring of swash motion (e.g. Guedes et al., 2011; Almar et al, 2017) and hence reflection (via the new predictor), and this has significant advantages over more conventional reflection measurement approaches which require costly in-situ marine deployments and are typically limited to relatively short durations (e.g. Baquerizo et al., 1997). In the current work, only a single cross-shore transect was analysed, however two-dimensional information on reflection can be obtained by extracting swash motion and As at several alongshore locations which may give new insight into the longshore variability of wave reflection and its effect on surf zone dynamics (Nicolae Lerma et al., 2017; Almar et al., 2018).

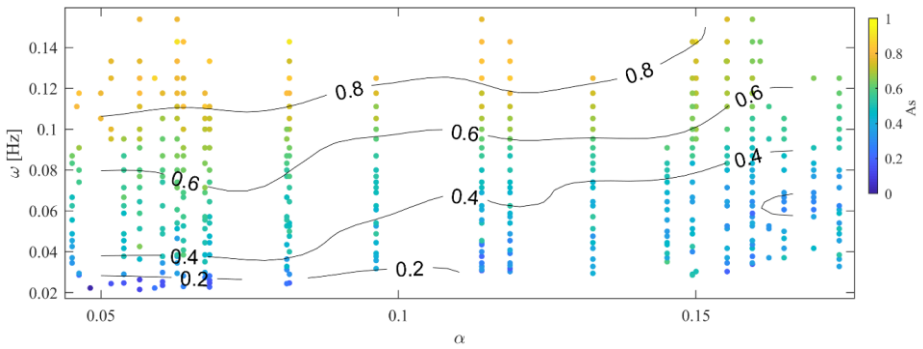

Figure 7: Distribution of runup asymmetry *As* as a function of swash frequency ω (inverse of individual swash duration) and active swash slope *α*. Dashed black contour lines represent iso-asymmetry levels.

5. Conclusions

A new predictor for wave reflection using video-derived runup asymmetry is proposed and applied to dissipative, intermediate and reflective beaches. A decomposition of the incoming wave energy fluxes into surf and swash zone dissipation and reflected waves showed that it is essential to account for swash-zone processes when estimating reflection, in particular at intermediate and reflective beaches. Our results show that runup asymmetry in uprush/backwash is correlated with swash dissipation: strong values of runup asymmetry indicate large swash-based energy dissipation. For our dataset, the new predictor based on remotely-sensed swash characteristics offers improved results (R^2=0.72) with better skill in comparison to conventional predictors based on surf similarity (R^2=0.38). This is because runup is the result of surf and swash zone wave transformation, and their interaction with the local morphology. In addition, it is shown that runup asymmetry reflects an equilibrium between swash period, slope and dissipation.

Acknowledgments

Mataquito exp. supported by Chilean CONICYT grants FONDECYT/1120878 and FONDAP/15110017, Grand Popo exp. by French INSU/CNRS EC2CO-LEFE/IRD, UNESCO co-chair ICPMA/IRHOB, and Nha Trang exp. by Vietnamese MOST (BKHCN/NDT-HD/2013/110) and MOST2: NDT.24.FRA/16. We are greatly indebted to the naval services of Benin at Grand Popo for their logistic support during the field experiment and for allowing the installation of the permanent video system on the semaphore. This research has received support from French grants through ANR

(COASTVAR: ANR-14-ASTR-0019). PAC also received support through CONICYT grants FONDECYT/1107415 and PIA/Basal FB0821.

References

Abdelrahman, S.M., Thornton, E.B., 1987. Changes in the short wave amplitude and wavenumber due to the presence of infragravity waves. Proceedings of the Specialty Conference on Coastal Hydraulics. American Society of Civil Engineers, New York, 458–478

Ahrens, J.P., 1979. Irregular wave runup, Coastal Struct.'79, Am. Soc. of Civ. Eng., New York, 998-1019

Almar, R., Cienfuegos, R., Gonzalez, E., Catalan, P.A., Michallet, H., Bonneton, P., Castelle, B., Suarez, L., 2012. Barred-beach morphological control on infragravity motion, International Conference on Coastal Engineering, Santander, Spain, 2-6 July 2012

Almar, R., Du Penhoat, Y., Honkonnou, N., Castelle, B., Laibi, R., Anthony, E., Senechal N., Degbe, G., Chuchla, R., Sohou, Z., Dorel, M., 2014a. The Grand Popo experiment, Benin, Journal of Coastal Research, 70, 651-656, ISSN 0749-0208

Almar, R., Michallet, H., Cienfuegos, R., Bonneton, P., Tissier, M.F.S., Ruessink, B.G., 2014b. On the use of the radon transform in studying nearshore wave dynamics. Coast. Eng. 92, 24–30

Almar, R., Almeida, P., Blenkinsopp, C., and Catalan, P., 2016. Surf-swash interactions on a low-tide terraced beach. Proceedings of the 14th International Coastal Symposium (Sydney, Australia). Journal of Coastal Research, Special Issue, 75, 348-352

Almar, R., Blenkinsopp, C., Almeida, L.P., Cienfuegos, R., Catalan, P., 2017. Wave runup video detection using the Radon Transform, Coastal Engineering, 130, 46-51

Almar, R., Nicolae Lerma, A., Castelle, B., Scott, T., 2018. On the influence of reflection over a rhythmic swash zone on surf zone dynamics. Ocean Dynamics, 68(7), 899–909

Bailard J.A., Devries, J.W., Kirby, J.T., 1992. Considerations in using Bragg reflection for storm erosion protection. Journal of Waterway, Port, Coastal and Ocean Engineering, 118, 62-86

Baldock, T.E., Holmes, P., 1999. Simulation and prediction of swash oscillations on a steep beach. Coast. Eng. 36, 219-242

Baquerizo, A., Losada, M.A., Smith, J.M. Kobayashi, N., 1997. Cross-shore variation of wave reflection from beaches J. Waterw. Port. Coast. Ocean Eng., 123, 274-279

Battjes, J., 1974. Surf similarity. 14th Coastal Engineering Conference, Am. Soc. Of Civ. Eng., Copenhagen, Denmark, 466–480

Battjes, J.A., Bakkenes, H.J., Janssen, T.T., van Dongeren, A.R., 2004. Shoaling of subharmonic gravity waves, J. Geophys. Res., 109, C02009, doi:10.1029/2003JC001863

Bergsma, E.W.J., Blenkinsopp, C.E., Martins, K., Almar, R. and Almeida, L.P., 2018. Observations and automated detection of bore-collapse using LiDAR measurements at Nha Trang beach, Vietnam. In revision for Continental Shelf Research

Blenkinsopp, C., Mole, M.E., Turner, I.L., Peirson, W.L., 2010. Measurements of the time-varying profile across the swash zone using an industrial LIDAR, Coastal Eng.,57, 1059-1065

Brocchini, M., Baldock, T.E., 2008. Recent advances in modeling swash zone dynamics: influence of surf–swash interaction on nearshore hydrodynamics and morphodynamics, Rev. Geophys., 46, p. RG3003

Carini, R.J., Chickadel, C.C, Jessup, A.T., Thomson, J., 2015. Estimating wave energy dissipation in the surf zone using thermal infrared imagery. J. Geophys. Res. Oceans, 120(6), 3937–3957, 10.1002/2014JC010561

Chen, X., Hofland, B., Uijttewaal, W., 2016. Maximum overtopping forces on a dikemounted wall with a shallow foreshore. Coastal Engineering 116, 89–102

Cienfuegos, R., Villagran, M., Aguilera, J.-C., Catalan, P., Castelle, B., Almar, R., 2014. Video monitoring and field measurements of a rapidly evolving coastal system: the river mouth and sand spit of the Mataquito river in Chile. Journal of Coastal Research, SI 70, 639–644

Davies, A.G., 1982. The reflection of water-wave energy by undulations on the seabed, Dynamics of Atmos. and Oceans, 6, 207–232

Davidson, M.A., Bird, P.A.D., Bullock, G.N., Huntley, D.A., 1996. A New Dimensional Number for the Analysis of Wave Reflection from Rubble Mound Breakwaters, Coastal Engineering 29, 93-120

Dee, D.P. et al., 2011. The ERA-Interim reanalysis: configuration and performance of the data assimilation system, Q. J. R. Meteorol. Soc., 137, 553–597, doi:10.1002/qj.828.

Diaz-Sanchez, R., Lopez-Gutierrez, J., Lechuga, A., Negro, V., Esteban, M., 2013. Direct estimation wave setup as a medium level in swash. Proceedings 12th International Coastal Symposium (Plymouth, England), Journal of Coastal Research, Special Issue, SI 65, 201–206

Dickson, W., Herbers, T.H.C., Thornton, E., 1995. Wave reflection from breakwater, J. of Water., Port, Coast., Ocean Eng., 121, 262-268

Elgar, S., Herbers, T., Guza, R., 1994. Reflection of ocean surface gravity waves from a natural beach. J. Physical. Oceanogr., 24(7), 1503–1511

Elgar, S, Guza RT. 1985. Observations of Bispectra of Shoaling Surface Gravity-Waves. Journal of Fluid Mechanics, 161:425-448

Elgar, S., Raubenheimer, B., Herbers, T.H.C., 2003. Bragg reflection of ocean waves from sandbars, Geophys. Res. Let.30, 1016, 10.1029/2002GL016351

Elfrink, B., & Baldock, T., 2002. Hydrodynamics and sediment transport in the swash zone: a review and perspectives. Coast. Eng., 45, 149-167.

Guard, P.A., Baldock, T.E., 2007. The influence of seaward boundary conditions on swash zone hydrodynamics. Coastal Eng., 54(4), 321–331

Guedes, R., Bryan, K., Coco, G., Holman, R., 2011. The effects of tides on swash statistics on an intermediate beach. Journal of Geophysical Research, 116, C04008

Guza, R.T., and Davis, R.E., 1974. Excitation of edge waves by waves incident on a beach. J. Geophys. Res. 79, 1285–1291

Guza, R.T., Bowen, A.J., 1976 Finite amplitude edge waves. J. Mar. Res. 34, 269–293

Guza, R., Thornton, E., 1982. Swash oscillations on a natural beach. J. Geophys. Res., 87, 483–491

Hancock, M.J., Landry, B.J., Mei, C.C., 2008. Sandbar formation under surface waves: Theory and experiments. Journal of Geophysical Research,113, C07022

Heikkila, J., Silven, O., 1997. A four-step camera calibration procedure with implicit image correction. Computer Vision and Pattern Recognition. In Proceedings of the IEEE Computer Society Conference, 1106–11012

Herbers, T.H.C., Lentz, S.J., 2010. Observing directional properties of ocean swell with an Acoustic Doppler Current Profiler (ADCP). Journal of Atmospheric and Oceanic Technology, 27, 210-225.

Holland, K.T. and Puleo, J., 2001. Variable swash motions associated with foreshore profile change, Journal of Geophysical Research, 106, C3, 4613-4623

Holland, K.T., Holman, R.A., 1993, The statistical distribution of swash maxima on natural beaches, J. Geophys. Res. , 87, 10, 271–10, 278

Holland, K., Holman, R., Lippmann, T., Stanley, J., Plant, N., 1997. Practical use of video imagery in nearshore oceanographic field studies. Oceanic Engineering, 22(1), 81–82

Holland, K.T., Holman, R.A. 1993. The statistical distribution of swash maxima on natural beaches. J. Geophys. Res., 98(C6), 10271–10278

Holland, K.T., Raubenheimer, B., Guza, R.T., Holman, R.A., 1995. Runup kinematics on a natural beach, J. Geophys. Res., 100, 4985-4993

Holman, R.A., 1986. Extreme value statistics for wave run-up on a natural beach, Coastal Engineering, 9 (6), 527-544

Holman, R.A., Sallenger, A., 1985. Setup and swash on a natural beach. J. Geophys. Res., 90, 945– 953

Hughes, S., Fowler, J., 1995. Estimating wave-induced kinematics at sloping structures. Journal of Waterway, Port, Coastal, and Ocean Engineering, 121(4), 209–215

Hughes, M.G., Masselink, G., Brander, R.W., 1997. Flow velocity and sediment transport in the swash zone of a steep beach, Marine Geology, 138, 91-103

Hughes, S., Mosseley, A. 2007. Hydrokinematic regions within the swash zone. Cont. Shelf Res., 27(15), 2000–2013

Inch, K., Davidson, M., Masselink, G., Russell, P., 2017. Observations of nearshore infragravity wave dynamics under high energy swell and wind-wave conditions, In Continental Shelf Research, 138, 2017, 19-31, ISSN 0278-4343

Iribarren, C., Nogales, C., 1949. Protection des ports. XVIIth International Navigation Congress, Section II, Communication, 31–80

Laibi, R., Anthony, E., Almar, R., Castelle, B., Senechal, N., 2014. Morphodynamic characterisation of the human-impacted Bight of Benin sand barrier coast, West Africa, Journal of Coastal Research, SI 70, 079-083, ISSN 0749-0208

Lefebvre, J-P., Almar, R., Viet, N., Uu, D., Thuan, D., Binh, L., Ibaceta, R., Duc, N., 2014. Contribution of swash processes generated by low energy wind waves in the recovery of a beach impacted by extreme events: Nha Trang, Vietnam. Journal of Coastal Research, SI 70, 663–668

Jeans, G., Primrose, C., Descusse, N., Strong, B., and van Weert, P., 2002. A Comparison between Directional Wave Measurements from the RDI Workhorse with Waves and the Datawell Directional Waverider, IEEE Seventh working Conference on Current Measurement Technology.

Krogstad, H.E., Gordon, R.L. and Miller, M.C., 1988. High-resolution directional wave spectra from horizontally-mounted acoustic Doppler current meters. J. Atmos. and Oceanic Technol., 5, 340-352

Martins, K., Blenkinsopp, C.E., Almar, R., Zang, J., 2017. The influence of swash-based reflection on surf zone hydrodynamics: a wave-by-wave approach. Coastal Engineering, 122, 27-43

Masselink, G., & Hughes, M., 1998. Field investigation of sediment transport in the swash zone. Cont. Shelf Res., 18, 1179-1199.

Mei, C.C., 1985. Resonant reflection of surface waves by periodic sand bars. J. Fluid Mech., 152, 315-335

Miche, R., 1951. Le pouvoir reflechissant des ouvrages maritimes exposes à l'action de la houle. Ann. Ponts Chaussees, 121, 285–319

513 Miles, J., Russell, P., 2004. Dynamics of a reflective beach with a low tide terrace. Continental Shelf
514 Research COAST3D Special Issue, 24, 1219–1247
515 Mizuguhi, M., 1984. Swash on a natural beach. Coastal Engineering Proceedings, 19, 2156–1028.
516 Muttray, M., Oumeraci, H., Ten Oever, E., 2006. Wave reflection and wave run-up at rubble mound
517 breakwaters, Proc. of ICCE, San Diego, California
518 Nicolae Lerma, A., Pedreros, R., Robinet, A., Sénéchal, N., 2017. Simulating wave setup and runup
519 during storm conditions on a complex barred beach. Coastal Engineering, 123, 29-41
520 O'Hare, T.J., Davies, A.G., 1993. Sand bar evolution beneath partially-standing waves: Laboratory
521 experiments and model simulations, Cont. Shelf Res., 13, 1149-1182
522 Power, H., Holman, R., Baldock, T., 2011. Swash zone boundary conditions derived from optical
523 remote sensing of swash zone flow patterns. J. of Geophysical Research, 116, 06007.
524 Puleo, J.A., Holland, K.T., 2001. Estimating swash zone friction coefficients on a sandy beach. Coastal
525 Eng., 43(1), 25–40
526 Raubenheimer, B., Guza, R.T., Elgar, S., Kobayashi, N., 1995. Swash on a gently sloping beach, J.
527 Geophys. Res.,100(C5), 8751–8760, doi:10.1029/95JC00232
528 Raubenheimer, B., Guza, R.T., Elgar, S., 1996. Wave transformation across the inner surf zone,J.
529 Geophys. Res.,101, 25, 589–25, 597,doi:10.1029/96JC02433
530 Rocha, M., Michallet, H., Silva, P., 2017. Improving the parameterization of wave nonlinearities—The
531 importance of wave steepness, spectral bandwidth and beach slope, Coastal Eng., 121, 77–89.
532 Ruessink, B.G., Kleinhans, M.G., van den Beukel, P.G.L., 1998. Observations of swash under highly
533 dissipative conditions, J. Geophys.Res.,103(C2), 3111–3118, doi:10.1029/97JC02791
534 Ruggiero, P., Komar, P.D., McDouglas, W.G., Marra, J.J., Beach, R.A., 2001. Wave runup, extreme water
535 levels and erosion of properties backing beaches. Journal of Coastal Research, 17 (2),407-419
536 Seelig, W.N., Ahrens, J.P., 1981. Estimation of wave reflection and energy dissipation coefficients for
537 beaches, revetments and breakwaters. CERC Technical paper 81-1, Fort Belvoir, U.S.A.C.E.,
538 Vicksburg, MS
539 Senechal, N., Coco, G., Bryan, K.R. Holman, R.A., 2011. Wave runup during extreme storm conditions,
540 J. Geophys. Res., 116 (7), p. C07032
541 Shen, M.C., Meyer, R.E., 1963. Climb of a bore on a beach part 3. run-up. J. Fluid Mech., 16, 113125.
542 Krogstad, H.E., Gordon, R.L. and Miller, M.C., 1988. High-resolution directional wave spectra from
543 horizontally-mounted acoustic Doppler current meters. J. Atmos. and Oceanic Technol., 5, 340-
544 352

Sheremet, A., Guza, R.T., Elgar, S., Herbers, T.H.C., 2002. Observations of nearshore infragravity waves: seaward and shoreward propagating components. J. Geophys. Res. 107, http://dx.doi.org/10.1029/2001JC000970. C8

~~Sheremet, A., R. Guza, S. Elgar, Herbers, T., 2001. Estimating infragravity wave properties from pressure-current meter array observations, paper presented at 27th International Conference on Coastal Engineering, Am. Soc. of Civ. Eng., Sydney, Australia~~

Strong, B., Brumley, B., Terray, E.A., Stone, G.W., 2000. The performance of ADCP-derived directional wave spectra and comparison with other independent measurements. OCEANS 2000 MTS/IEEE Conference and Exhibition. Conference Proceedings, DOI: 10.1109/OCEANS.2000.881763

Sutherland, J., O'Donoghue, T., 1998. Characteristics of wave reflection spectra. J. Waterw. Port Coastal Ocean Eng., 124(6), 303–311

Tatavarti, R.V., Hunfley, D.A., and Bowen, A.J., 1988. Incoming and outgoing wave interactions on beaches, Proceedings of the 21 Coastal Engineering Conference, American Society of Civil Engineers, 1, 136-150

Vousdoukas, M.I., 2014. Observations of wave run-up and groundwater seepage line motions on a reflective-to-intermediate, meso-tidal beach. Marine Geology 350. DOI: 10.1016/j.margeo.2014.02.005

Whitham, G.B., 1958. On the propagation of shock waves through regions of non-uniform area of flow. J. of Fluid Mechanics 4, 520-539

Yu, J., Mei, C.C., 2000. Formation of sand bars under surface waves. J. Fluid Mech. 416, 315–348

Formatted: French (France)